Results in Engineering 23 (2024) 102558

Contents lists available at ScienceDirect

Results in Engineering

journal homepage: www.sciencedirect.com/journal/results-in-engineering

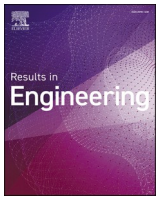

Coupled injection moulding simulation–thermal and mechanical simulation method to analyse the operational behaviour of additively manufactured polymeric injection moulds

Szabolcs Krizsma [a], Péter Széplaki [a], András Suplicz [a,b,*]

[a] Department of Polymer Engineering, Faculty of Mechanical Engineering, Budapest University of Technology and Economics, Műegyetem rkp. 3., H-1111, Budapest, Hungary
[b] MTA-BME Lendület Lightweight Polymer Composites Research Group, Műegyetem rkp. 3., H-1111, Budapest, Hungary

ARTICLE INFO

Keywords:
Rapid tooling
Injection moulding
Powder bed fusion
Injection moulding simulation
Coupled simulation

ABSTRACT

The appearance and the widespread application of additive manufacturing (AM) technologies has brought a sweeping change to the polymer processing industry. Hybridization of the technologies like printing moulds for conventional injection moulding opens new opportunities because parts can be manufactured in low volumes fast and cost effectively. This way, the greatest limitation of injection moulding can be overcome, which is economic viability only at large-volume production. We manufactured a low-volume mould insert from a polyamide powder with a Powder Bed Fusion (PBF)–based technology: Selective Laser Sintering (SLS). We performed material tests to determine the stiffness and the creep compliance of the material in the relevant temperature region. These parameters determine the suitability of the material for prototype mould making and they are inputs for the simulation of prototype moulds. We also applied comprehensive measurement technology consisting of simultaneous strain, temperature and cavity pressure measurement to get a broad view of the operational behaviour of the insert. We introduced a novel coupled simulation method, which can forecast the thermal and deformational state of the SLS-printed mould insert during operation. This coupled method first uses injection moulding simulation to create the mould mesh and to calculate the transient pressure and temperature fields during operation. The results are then exported to a finite element mechanical simulation, where a transient thermal and then a structural simulation is run. The transient thermal simulation is necessary to calculate the temperature field of the mould components, while the structural simulation requires the pressure load input from the injection moulding simulation and the temperature field from the transient thermal simulation. Our simulation method proved suitable for modelling the operational behaviour of polymeric mould inserts.

1. Introduction

Additive manufacturing (AM) has already brought tremendous change to injection moulding. Powder bed fusion (PBF) technologies like selective laser sintering (SLS) allow the printing of high-performance technical polymers like polyamide. The mechanical properties of polyamide and its glass transition temperature is among the best that polymers can deliver. AM can produce very complex final parts and moulds in a single technological step without the large investment cost of conventional mould making. The hybridization of injection moulding with AM moulds and part inserts has the potential to deliver outstanding results. Mass customisation and cost-effective low-volume production of injection moulded parts become reality by using the potential of AM [1].

Additively manufactured metallic injection moulds can be used for large-volume production. These moulds are made by PBF processes that make feasible complex and freeform geometries like conformal cooling channels. The use of conformal cooling increases cooling efficiency, which leads to a significant reduction in cycle time and enhanced productivity. Feng et al. [2] made a thorough review of the designing, manufacturing and application of conformal cooling. One of their conclusions was that laser powder bed fusion (LBPF) is a popular and practical technology to produce conformal cooling in a wide variety of different geometries. Kuo et al. [3] compared different conformal cooling channel profiles and layouts printed into injection mould inserts

* Corresponding author. Department of Polymer Engineering, Faculty of Mechanical Engineering, Budapest University of Technology and Economics, Műegyetem rkp. 3., H-1111 Budapest, Hungary.
E-mail address: suplicz@pt.bme.hu (A. Suplicz).

https://doi.org/10.1016/j.rineng.2024.102558
Received 21 March 2024; Received in revised form 8 July 2024; Accepted 11 July 2024
Available online 14 July 2024

made from maraging steel. They achieved a significant reduction in cycle time, proving the efficiency of conformal cooling. Kirchheim et al. [4] also applied conformal cooling to enhance the cooling performance of a mould insert made from maraging steel. The combination of conformal cooling channels and variotherm mould tempering leads to substantial cycle time reduction and an enhanced surface quality of the product. Ben Slama et al. [5] showed that injection moulding simulation can be an ideal tool to design a wide range of different conformal cooling channel layouts that can enhance the cooling efficiency of critical areas in an injection mould. Ilyas et al. [6] printed conformally cooled mould inserts from polymer-coated metal powder and then sintered the part and applied surface finishing. They proved that SLS printing can also be used to make conformally cooled metallic mould inserts. Bai et al. [7] analysed the dimensional accuracy of a conformally cooled steel injection mould insert produced by selective laser melting (SLM). They found that the mould insert can meet geometric and surface quality requirements after heat treatment and surface finishing. The modification of surface hardness is an intensively researched topic for SLM printed parts [8]. Török et al. [9] applied a hybrid approach, where they printed the shell of a mould insert by LBPF from maraging steel. Then, they cast molten copper into this steel shell to enhance the thermal conductivity of the mould insert. They managed to reach an additional 15 % residual cooling time reduction with their hybrid mould compared to the LPBF-printed, conformally cooled steel mould. Saifullah et al. [10] inserted high thermal conductivity copper tubes inside a steel mould to improve cooling efficiency. They achieved a cycle time reduction of 35 % compared to conventional cooling channels. Naranjo et al. [11] created and characterised a feedstock containing precipitation hardened stainless steel (17-4 PH) that can be processed both by fused filament fabrication (FFF) and metal injection moulding. These feedstocks allow the printing of metallic parts without the expensive and rare LBPF metal printers.

Alongside conformal cooling, another development direction of freeform geometries are lattice structures [12]. Additive technologies can manufacture highly complex, freeform geometries created by advanced computer aided design (CAD) systems [13]. They allow significant weight saving compared to solid geometries, while retaining a significant amount of strength and stiffness. Park et al. [14] used a Ti–6Al–4V powder to print injection mould inserts with lattice structures. They achieved a 79 % weight reduction compared to the solid mould insert, and used the printed inserts throughout 400 injection moulding cycles successfully. Weight reduction of injection moulds can lead to decreased energy consumption and more sustainable production. Mahshid et al. [15] also used PBF technology to print steel inserts with different lattice structures inside them. They compared the structures based on their compressive strength and introduced a modelling technique to estimate the load-bearing capacity of these structures. Chantzis et al. [16] also applied lattice structures to enhance the cooling performance of a hot stamping die. Tan et al. [17] inserted supporting lattice structures into large-diameter conformal cooling channels to make them printable by LPBF. The injection mould insert with higher diameter conformal cooling channels showed enhanced cooling efficiency.

Additive manufacturing is also gaining ground in the production of polymeric moulds for low-volume injection moulding. The most popular additive technologies for non-thermoplastic resins are Material Jetting (MJ) (including PolyJet) and Vat photopolymerisation (including stereolitography, SLA) while thermoplastic parts are typically processed by Material Extrusion (ME), including Fused Filament Fabrication (FFF) or powder-based technologies like Selective Laser Sintering (SLS). Mendible et al. [18] compared the thermal state and the operational deformation of a machined and a DMLS-printed steel insert with a PolyJet printed insert. They found that the polymeric mould insert heated significantly more and showed more than an order of magnitude higher operational deformation than the metal inserts. Minetola et al. [19] compared the geometric tolerance capabilities of three different AM technologies for polymers: FFF, SLS and the Arburg Freeformer method. They found that the best ISO tolerance grades were reached by the FFF printer but the SLS and the Arburg Freeformer printers showed quite similar dimensional accuracy. They generally concluded that the dimensional accuracy of the printed parts heavily depend on the minimal layer thickness of printing.

Thermal load has a determining role in the lifetime and applicability of polymeric moulds. It is crucial to keep polymeric mould inserts below their glass transition temperature (T_g). Zink et al. [20] compared different cooling channel layouts in PolyJet-printed mould inserts. They found that conformal cooling reduced the time required for the mould insert surface to cool below the glass transition temperature by 70 % compared to conventional cooling or no cooling. Printing orientation and the resulting delamination has a fundamental role in the lifetime of Material Jetting printed photopolymer injection mould inserts [21,22]. Davoudinejad et al. [23] demonstrated the negative effect of thermal cycling on the lifetime of vat photopolymerisation-printed mould inserts. Thermal aging increased the crack propagation speed of mould inserts significantly and reduced their longevity. Bagalkot et al. [24] identified the main injection moulding parameters that determine the longevity of a PolyJet-printed mould (made from DigitalABS). These parameters were: mould temperature, injection pressure, injection speed, holding pressure and cooling time. They outlined an algorithm to set these parameters properly to increase mould lifetime. Krizsma et al. [25,26] presented a novel comprehensive measurement system of prototype injection moulds to measure their operational deformations and their thermal state. Such a measurement system helps to adjust the injection moulding parameters and maximise mould insert lifetime.

Selective laser sintering (SLS) is a promising AM technology as it allows the printing of high-performance polymers, mainly polyamide [27,28]. The printing process has already been analysed in-depth by Soldner et al. [29], who modelled the thermal conditions and crystallisation kinetics of PA12 during printing. Salazar et al. [30] compared the mechanical behaviour of injection moulded and SLS-printed PA12 under static and fatigue load. SLS-printed PA12 showed higher surface roughness and porosity compared to injection moulded PA12. SLS-printed specimens showed slightly higher modulus of elasticity while less than half or one sixth of the elongation at break (depending on the printing direction) of the injection moulded PA12. A significant challenge of SLS printing is the dimensional stability of the printed part. Dastjerdi et al. [31] presented a finite element modelling-based optimisation algorithm to minimise the shrinkage and warpage of parts manufactured from PA12 by SLS. Kampker et al. [32] created a comparative study of a PA3200GF (Polyamide 12 with glass beads) injection mould (produced by SLS), a DigitalABS mould (produced by PolyJet) and a conventional machined aluminium injection mould. The SLS-printed mould showed the highest surface roughness while size deviations were minimal after the injection moulding series; this indicates the durability of the mould. The tensile specimens injection moulded into the PA3200GF mould showed considerably higher modulus of elasticity while lower elongation at break. This can be attributed to the different crystallisation behaviour due to the low thermal conductivity and the resulting slow cooling compared to the aluminium mould.

Alongside the appearance of additive technologies and the rise of rapid tooling, another significant trend of injection moulding is the spread of measurement technology. Special injection moulding techniques like rapid heat cycle moulding (RHCM) are based on the strict measurement and regulation of the mould cavity surface temperature. RHCM allows the reduction of the required hydraulic pressure, thus saving energy while it can also eliminate moulding defects like warpage [33]. Infrared thermal imaging camera measurements allow the melt flow visualisation during injection moulding that is especially helpful to improve the surface quality and dimensional accuracy of the moulded parts [34]. The finite stiffness of moulds and moulding machine components lead to operational deformations. Mahshid et al. [35] applied

eddy-current displacement sensors to measure the operational deformations of mould components. Zhao et al. [36] set up a novel ultrasonic measurement method to monitor the clamping force acting on the tie bar of the injection moulding machine. Cavity pressure measurement is also used for product quality monitoring [37,38]. The simulation of injection moulding is also an intensively researched area because it allows the analysis of the operational deformations and the thermal state of injection moulds. Research has already been carried out to properly validate the results of injection moulding simulation. Special glass mould designs allow the monitoring of the melt flow front by high-speed camera during injection moulding [39,40] Tosello et al. [41] used injection pressure and time, the shape of the flow front, and short shot products to validate their simulation model of a micro injection moulding process. Davoudinejad et al. [42] created a coupled thermal and mechanical simulation to analyse the thermal state and the deformations of a vat photopolymerisation printed prototype injection mould. Abbés et al. [43] built a finite element thermal simulation to model the temperature distribution of a conformally cooled mould insert. Simulation helped to optimise conformal cooling and reduce injection moulding cycle time. Mazur et al. [44] thoroughly validated the accuracy of cooling simulation with actual injection moulding measurements. They compared a conventionally cooled mould insert with an insert SLM-printed from H13 tool steel. They found that injection moulding simulation is a suitable tool to model the thermal state of the mould but improvements can be made especially when modelling additively manufactured mould inserts.

There is already a significant amount of accumulated experience on the applicability of prototype injection moulds. However, the possibilities of modern measurement technology are not exploited to the fullest and the exact operational state of prototype moulds is still largely unknown. Systematic modelling and design of additively manufactured moulds is rare. This research article aims to fill the knowledge gaps in the field of comprehensive measurement technology of prototype injection moulds as well as creating a novel coupled simulation approach to accurately model the operational deformation and temperature of additively manufactured moulds.

This research article presents a novel coupled simulation method that allows the finite element modelling of polymeric prototype injection moulds. Material testing was carried out first including the conventional dynamic mechanical analysis (DMA) and the creep testing of the material. It was to determine the stiffness of the material as a function of temperature and to measure the time dependent (creep) behaviour of the material. After that, injection moulding tests were performed and the operational strains and temperatures were measured at different holding pressures levels. Following the measurements, a novel coupled simulation method was outlined that is a combination of injection moulding simulation, transient thermal and structural simulation. The material parameters for the creep models of the mechanical simulations were calibrated by a small model that simulates the creep tests. Following that, the injection moulding simulation model was built in Autodesk Moldflow and its transient pressure results and the finite element mesh of the mould components were exported to Ansys Workbench. The thermal and mechanical simulations were then performed in Ansys. Both the temperature and the strain results of the simulations were successfully validated by the actual measured results, proving the adequacy of the presented modelling method. The outlined coupled modelling method is novel and it has evident practical benefits as it allows the accurate modelling of low-volume mould inserts and part inserts.

2. Materials and methods

2.1. Mould insert and sample preparation

Dynamic mechanical analysis (DMA) specimens were printed from PA2200 (Polyamide 12) powder manufactured by EOS GmbH (Germany, Krailling). The inserts were printed by an SLS sPro 60 HD printer manufactured by 3D Systems (United States, Rock Hill). The specimens had the dimensions of 4 × 10 × 59 mm. Table 1 shows the mechanical and thermal properties of PA2200. The material grade has acceptable strength, stiffness and has outstanding resistance against heat, indicated by the high Vicat softening temperature. The thermal conductivity of the material is low, while the specific heat and coefficient of thermal expansion are high, which is general for polymers. These thermal properties indicate that a relatively long idle time has to be kept during the injection moulding tests because the insert will heat rapidly.

2.2. Material testing

The printed specimens were analysed with a TA Instruments (USA) Q800 dynamic mechanical analyser (DMA). The DMA analysis determined the creep compliance at different temperatures (in creep time temperature superposition (TTS) mode). The measurement parameters are listed in Table 2. The analysed temperature range was chosen to completely cover the application temperature range of the mould insert.

The temperature dependence of stiffness was also measured by DMA in Multi-Frequency–Strain mode and the tests were performed with the dual cantilever clamp. The analysed temperature region was 25–105 °C, and the loading frequency was 1 Hz. Heating speed was 3 °C/min and the amplitude of loading was 15 μm.

2.3. The comprehensive state monitoring of mould inserts

We presented the state monitoring system in-depth in Refs. [25,26]. Fig. 1 shows the test mould. The dimensions of the injection mould insert were 75 × 65 × 15 mm while those of the injection moulded plate were 65 × 55 × 2 mm. The mould was filled through a 1 mm thick edge gate. The state monitoring of the prototype mould consists of two strain gauges (KMT-LIAS-06-3-350-5EL, Hungary) glued into the slots at the back of the insert and a thermocouple (Heraeus M222 Pt100, Heraeus Holding GmbH, Germany). The measured strain data were collected by a Spider 8 unit (Hottinger Baldwin Messtechnik GmbH, Austria), while the temperature data were gathered by an Ahlborn Almemo 8990–6 data collector unit (Ahlborn Mess-und Regelungstechnik GmbH, Germany). The surface temperature was measured by a FLIR A325sc thermal imaging camera (Teledyne FLIR LLC, Wilsonville, United States). We analysed the accuracy of the printing and the residual deformations by scanning the mould insert before and after the injection moulding series. We used a GOM ATOS Core 5 M scanner (Carl Zeiss GOM Metrology GmbH, Germany) whose theoretical resolution is 0.01 mm.

We used a polypropylene homopolymer: Tipplen H145F (MOL Group Plc., Hungary) for the injection moulding tests. 'The injection moulding of this material produces an acceptable temperature and pressure load on the mould insert. The products were injection moulded with an Arburg Allrounder Advance 270S 400-170 (ARBURG GmbH, Germany) machine (screw diameter: 30 mm). The main injection moulding parameters are shown in Table 3. Keeping a low injection rate and pressure limit is essential to protect the mould insert from excessive pressure load. By keeping a low injection rate, the clamping force can also be

Table 1
Material properties of PA2200 (Polyamide 12).

Properties	Unit	Typical value
Tensile strength	MPa	48
Tensile modulus	GPa	1.65
Flexural modulus	GPa	1.5
Elongation at break	%	18
Vicat softening temperature (50 °C/h 50 N)	°C	163
Thermal conductivity	W/(m·K)	0.144
Specific heat	J/(kg·K)	2350
Coefficient of thermal expansion	1/K	~$1.09 \cdot 10^{-4}$

Table 2
Parameters of DMA creep TTS testing.

Parameters used	Unit	Typical value
Furnace time	min	10
Creep time	min	30
Recovery	min	30
Minimum temperature	°C	30
Maximum temperature	°C	90
Temperature increment	°C	5
Bending stress	MPa	5
Atmosphere	Air	

minimised, which increases the lifetime of the mould insert. Due to the relatively low thermal conductivity of the polyamide tool insert material, the solidification of the product is slow, which increases product shrinkage. A longer holding time is needed to compensate for this, and a longer residual cooling time is also necessary for a proper ejection temperature. A long idle time is also necessary for the mould insert so that it can cool down and early failure can be prevented.

2.4. Finite element modelling of the operational state of the mould insert

Following the injection moulding tests, a coupled injection moulding simulation – finite element mechanical simulation method was elaborated to model the thermal and deformational state of the mould insert during operation. Injection moulding simulation was built in Moldflow while the thermal and structural simulations were built in Ansys Workbench.

3. Results and discussion

3.1. Material testing

3.1.1. Dynamic mechanical analysis

The storage modulus (E') and the loss factor (d) were determined by conventional DMA. We performed a temperature sweep to characterise the temperature dependence of stiffness (Fig. 2). A gradual decrease can be observed in the storage modulus from 1340 MPa measured at 26 °C down to 340 MPa at 100 °C. The storage modulus measured at room temperature is close to the flexural modulus indicated on the datasheet of the material (Table 1). The minor plateau observed in the loss factor (approximately between 35 °C and 65 °C) does not indicate significant changes in the material in the analysed temperature region (between 25 °C and 100 °C).

3.1.2. Creep tests

Creep is the primary source of deformation for polymeric injection moulds and inserts. Creep is especially relevant at higher temperatures that can occur during the operation of the injection mould. Creep testing was also performed on DMA in creep time–temperature superposition (TTS) mode. Creep compliance (J), which characterises the material's tendency to creep, can be calculated with Eq. (1), where (ε_{fl}) is the time-dependent flexural strain and (σ_0) is the pre-set flexural stress.

$$J(t) = \frac{\varepsilon_{fl}(t)}{\sigma_0} \tag{1}$$

Table 3
The injection moulding parameters.

Processing parameters	Unit	Value
Clamping force	t	5
Dose volume	cm^3	40
Injection rate	cm^3/s	15
Injection pressure limit	bar	500
Switchover point	cm^3	26
Holding pressure	bar	50 to 300
Holding time	s	15
Residual cooling time	s	30
Cycle time (from mould closing to mould opening)	s	~56.6
Overall cycle time (delay time included)	s	300
Melt temperature	°C	190
Initial mould temperature	°C	31 (unheated mould)

During the injection moulding test, 10 cycles were moulded at a holding pressure of 75 bar first. This was followed by an increasing holding pressure section, where the holding pressure was increased from 50 bar to 300 bar by 25 bar in every second cycle. After that, additional 10- cycle repeatability tests were performed at 125 bar, 175 bar and 225 bar.

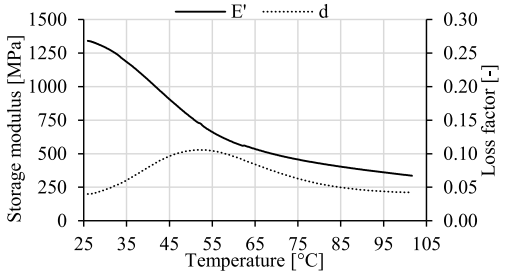

Fig. 2. Storage modulus (E′) and loss factor (d) of the insert material measured by DMA.

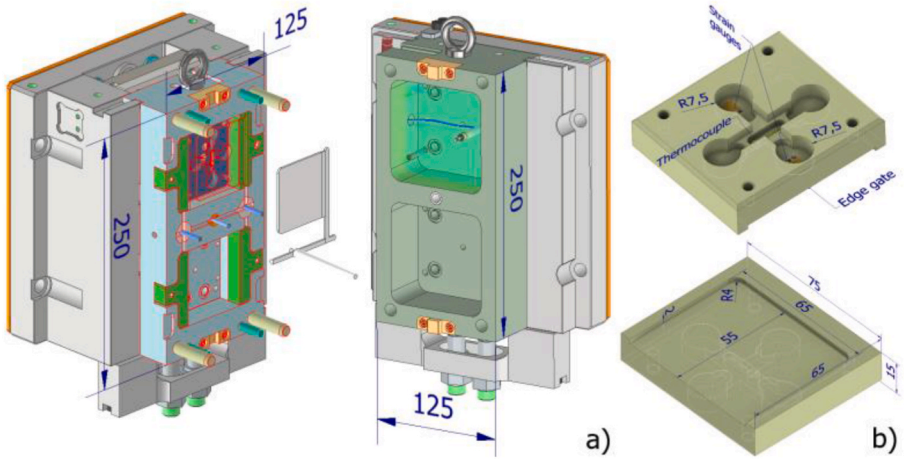

Fig. 1. The test mould and the product a), the moving side insert with the strain gauges and the thermocouple b).

The creep compliance results are presented in Fig. 3. The maximal creep compliance (measured right before unloading) shows a gradually increasing tendency and no stepwise increases can be observed, which is highly benefical for the applicability of the material. The maximal creep compliance is 1480 $\mu m^2/N$ at 30 °C, which increases to 3160 $\mu m^2/N$ at 110 °C. It is a narrowly more than a twofold increase in the entire analysed temperature region. The analysed temperature range covers the entire temperature range of application of the injection mould insert.

3.2. 3D scanning the mould insert before and after the injection moulding series

The mould insert was 3D scanned both in as-printed state and after the injection moulding series. The scanned geometries were compared with the nominal three dimensional geometry and the results are presented in Fig. 4. The first scanning characterises the dimensional accuracy of the printing while the second scan highlights the operational deformations occurring during injection moulding. The insert shows acceptable dimensional accuracy of the cavity surface as the maximal size deviations are below 0.1 mm for the entire cavity surface both in as-printed state and after the injection moulding series. Size deviations in the corner points of the insert indicate no significant warpage of the part. However, volumetric shrinkage can be observed at the surface in contact with the edge gate insert. A maximal deviation of −0.47 mm can be found in as-printed state that grew to −0.88 mm on the side of the insert after the injection moulding series. It is because the presence of a gap between the cavity insert and the gate insert results in the cyclic occurrence of flash that further deforms the insert. The maximal, −0.88 mm deformation can be located where the melt first enters the cavity, therefore its pressure is highest at that location. The −0.62 mm deformation at the end of the edge gate is also significant. These negative size deviations can be traced back to the shrinkage of the mould insert that has to be compensated by scaling up the geometry prior to printing. By comparing the scanning results before and after the injection moulding series, it is clear that the cavity surface only suffered negligible deformation meaning that the mould insert can be used for stable and repeatable production. It also has to be noted that the surface of the mould insert is rough. It is because the layer thickness of the printing is 120 μm that is considerably high.

3.3. Injection moulding tests

3.3.1. Repeatability test at a constant holding pressure of 75 bar

We started injection moulding at a constant holding pressure of 75 bar and injection moulded 10 cycles to characterise the stability and the reproducibility of the process. The strain results are presented in Fig. 5. Maximal operational strain reached 0.15 % at the start of the holding phase, which falls to −0.09 % in the holding phase. It is because the 75 bar holding pressure is considerably low compared to the maximal injection pressure of ~320 bar at switchover. The low holding pressure cannot compensate for product shrinkage properly, which results in a sharp drop of strain as the mould insert springs back in the free space. After the holding phase, strain begins to rise again because the heat is transferred from the solidifying product to the mould insert. The transferred heat causes thermal expansion and increased creep compliance, which cause an increase in strain. The expanding insert also compresses the product, which results in a sharp increase in strain as the clamping force is removed and the part is ejected. After the ejection of the part, the idle time begins, where the mould insert can expand out of the parting plane. As the entire volume of the mould insert reaches a uniform temperature and begins to cool down, the operational strains also decrease. The injection moulding process can be considered stable, as the operational deformations show little scatter. The yellow curve is related to the first cycle, from which the next cycles started to be more reliable because the mould has reached a more stable condition by the combined effect of the clamping force and the injection pressure.

3.3.2. Injection moulding with increasing holding pressure

The injection moulding series was continued with the increasing holding pressure section. We started moulding parts at a holding pressure of 50 bar and increased it by 25 bar in every second cycle to 300 bar. The strain results are presented in Fig. 6. With this segment of the injection moulding series we determined the pressure limit for the applicability of the mould. As holding pressure increased, so did maximal strain and the strains also stabilised at a higher value in the holding and in the residual cooling phases. A larger, stepwise decrease can also be observed at mould opening, indicating the overfilling of the cavity. The operational strains are slightly higher near the gate than far from the gate because the pressure drops as the melt fills the cavity. The generally applied clamping force of 5 tons was insufficient at 275 bar holding pressure and the mould opened partially. Therefore, the clamping force was increased to 10 tons when injection moulding with 300 bar holding pressure.

3.3.3. Repeatability tests at elevated holding pressures

Following the increasing holding pressure section, we carried out repeatability tests at additional elevated holding pressures: at 125 bar, 175 bar and 225 bar. The operational strain is presented for the location near the gate at the three different holding pressures in Fig. 7. The strain curves also show little scatter indicating the stability of the technology. 10 cycles were injection moulded at each holding pressure and the strain results are presented in Fig. 7.

3.3.4. Operational temperature of the mould inserts

The surface temperature and the volumetric temperature of the insert were measured with a thermal imaging camera and a thermocouple, respectively. (Figs. 8 and 9). The surface temperature of the mould insert was measured in the idle times between the cycles when the mould was opened and the part was ejected. The thermal imaging camera was placed next to the injection moulding machine and it viewed the polymeric mould insert through the open door of the moulding machine. The surface temperature of the insert fluctuates between 53 °C

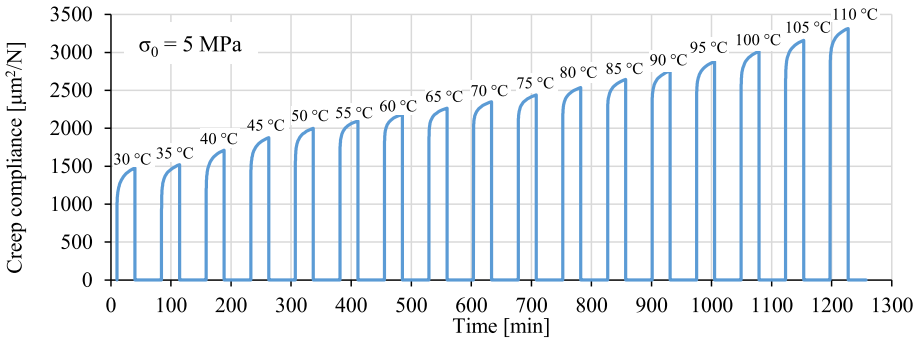

Fig. 3. Creep compliance of the insert material in the 30–110 °C temperature range measured by DMA Creep TTS.

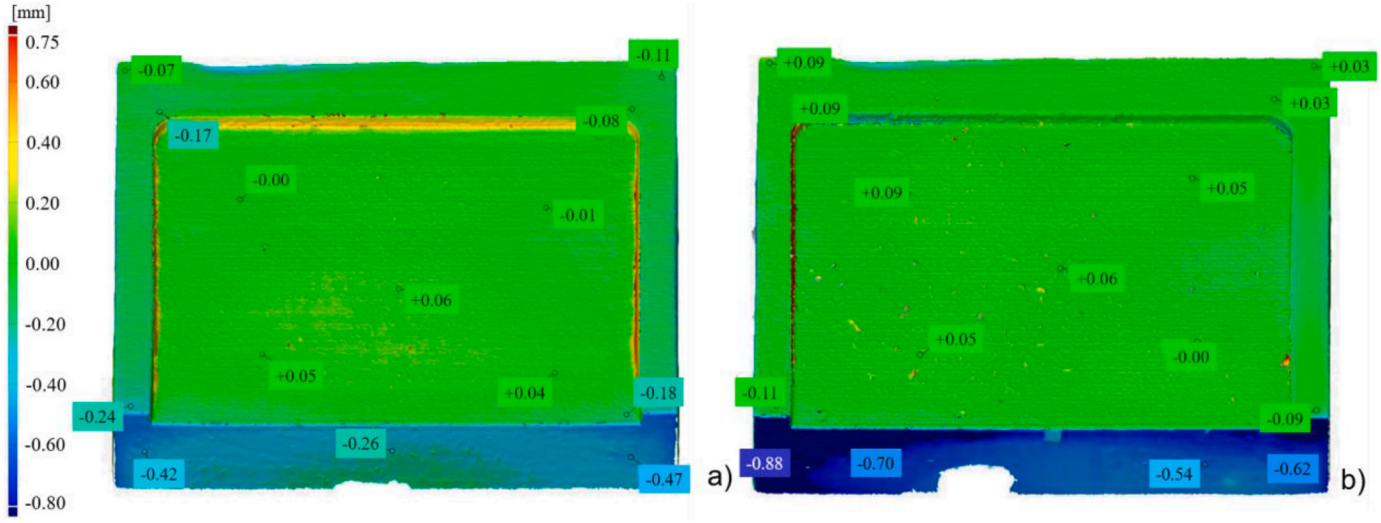

Fig. 4. 3D scanning result of the mould insert in as-printed state a) and after the injection moulding series b).

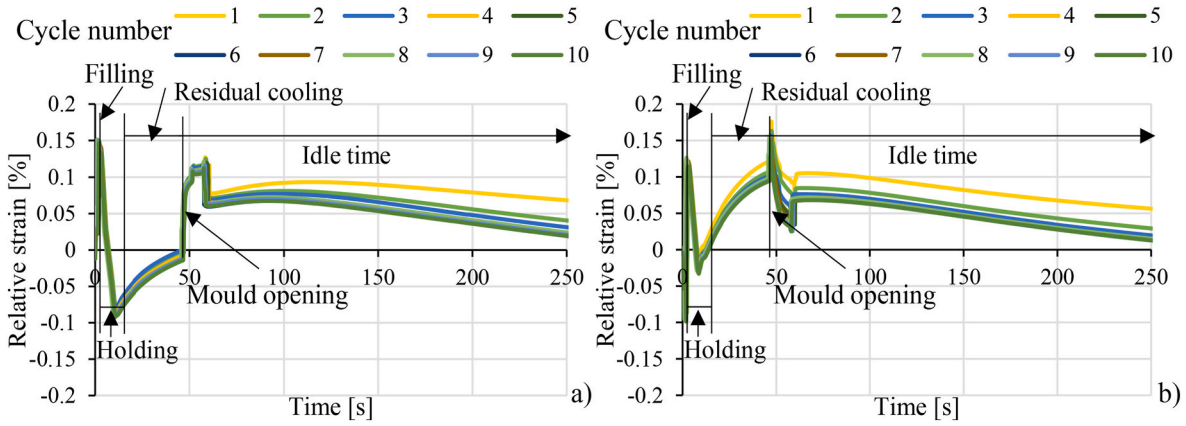

Fig. 5. Operational strain of the mould insert at a constant holding pressure of 75 bar: near the gate a) and far from the gate b).

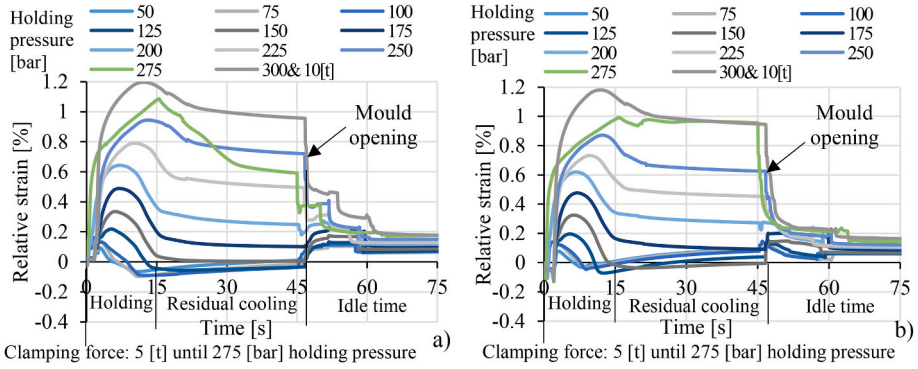

Fig. 6. Operational strain of the mould insert at increasing holding pressure: from 50 to 300 bar at the slot near the gate a) and far from the gate b).

at mould opening and 43 °C at the end of the idle time at a holding pressure of 75 bar. As holding pressure increased, so did cavity surface temperature and steeply increasing temperatures can be observed at mould opening and at the end of the idle time. This is due to the fact a higher holding pressure results in an improved heat transfer coefficient between the melt and the cavity, therefore heating of the insert becomes more intense. The heat transfer coefficient grows between two surfaces as the contact pressure increases between them. An elevated holding pressure also results in an increased amount of injected melt, causing an additional heat load to the mould insert. A maximal surface temperature of 80 °C (at mould opening) was reached at the highest holding pressure of 300 bar. As holding pressure fell to 125 bar, so did maximal surface temperature. At the 125 bar repeatability test, the maximal surface temperature stabilised at 56 °C, which grew to 60 °C at a holding pressure of 175 bar and to 65 °C at a holding pressure of 225 bar. These temperature results prove that the operational heat load is in an acceptable range, as the Vicat softening temperature (163 °C at 50 °C/h and 50 N) of the material is well above these values.

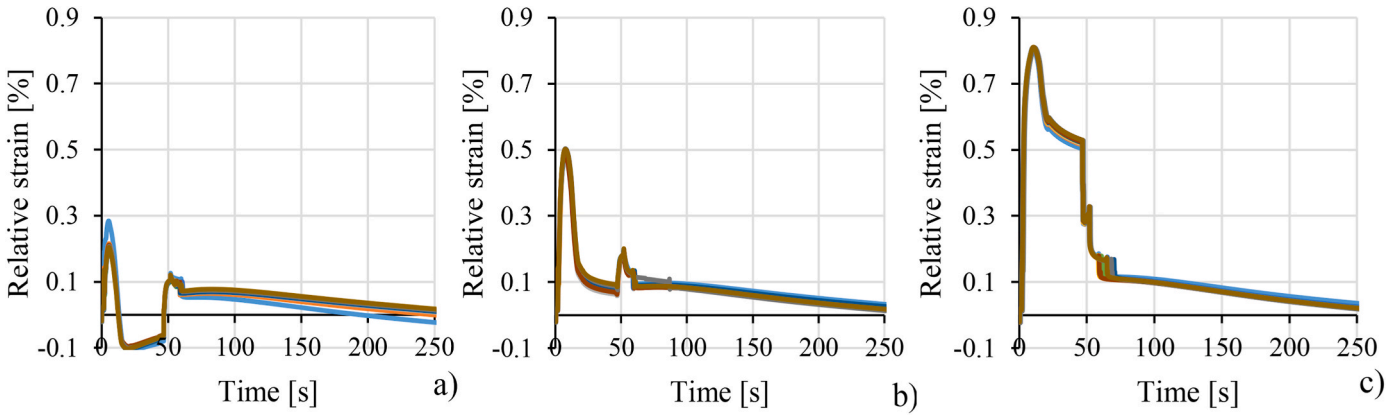

Fig. 7. Operational strain of the injection mould insert near the gate at a holding pressure of 125 bar a), 175 bar b) and 225 bar c).

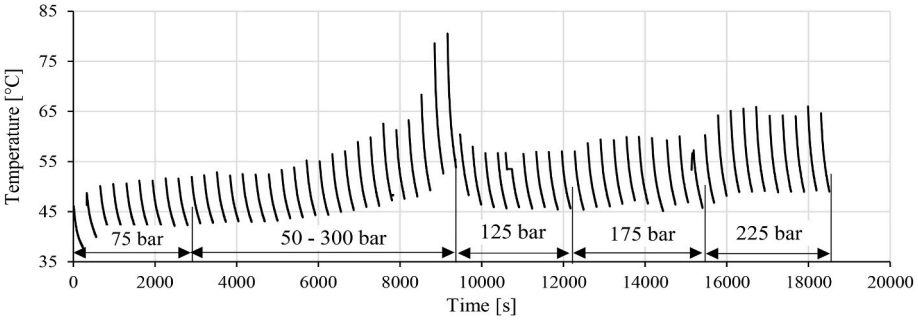

Fig. 8. Surface temperature of the mould insert measured with a thermal imaging camera.

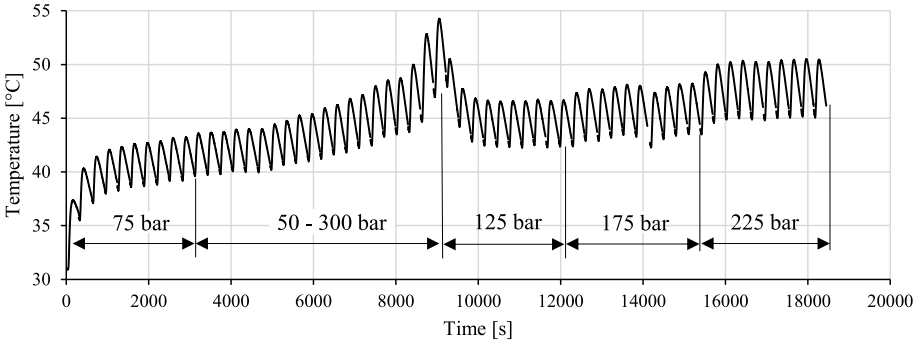

Fig. 9. Volumetric temperature of the mould insert measured with a thermocouple.

The temperature at the back of the insert was also measured with a thermocouple. The temperature oscillates during the injection moulding cycles. The tendency of volumetric temperature follows that of the cavity surface and maximal volumetric temperature is also reached at a holding pressure of 300 bar. The maximum surface temperature at a holding pressure of 300 bar is 80 °C while the maximum temperature at the back of the insert is just 54 °C, due to the low thermal conductivity of the insert material. It is a 26 °C temperature drop in a wall thickness of just 6 mm.

3.4. Simulation of the polymeric mould inserts

Following the material tests and the injection moulding series, we developed a novel coupled simulation approach that combines injection moulding simulation with finite element thermal and structural simulation to model the operational state of the polymeric injection mould. Fig. 10 shows the flowchart of the coupled injection moulding simulation–finite element thermal and mechanical simulation. The analysis begins with the preparation of the model in the injection moulding simulation software (Moldflow Insight). The mould and the product have to be meshed and the basic process parameters (mould and melt temperature, flow rate, switchover point, holding pressure and time, and residual cooling time) have to be set. Following that, the injection moulding simulation has to be run and the necessary data (mould mesh, and time-dependent pressure and temperature load) have to be exported to the finite element simulation software (Ansys Workbench). For that, a proper input file has to be generated. The data then have to be imported into the mechanical simulation software and a transient thermal analysis has to be run to calculate the time-dependent temperature field of the part and the surrounding mould components. This thermal analysis requires additional material properties of the mould components and the part, including density, the coefficient of thermal expansion, and specific heat. These data can be determined by material testing (DSC and thermal conductivity measurement) or they can be

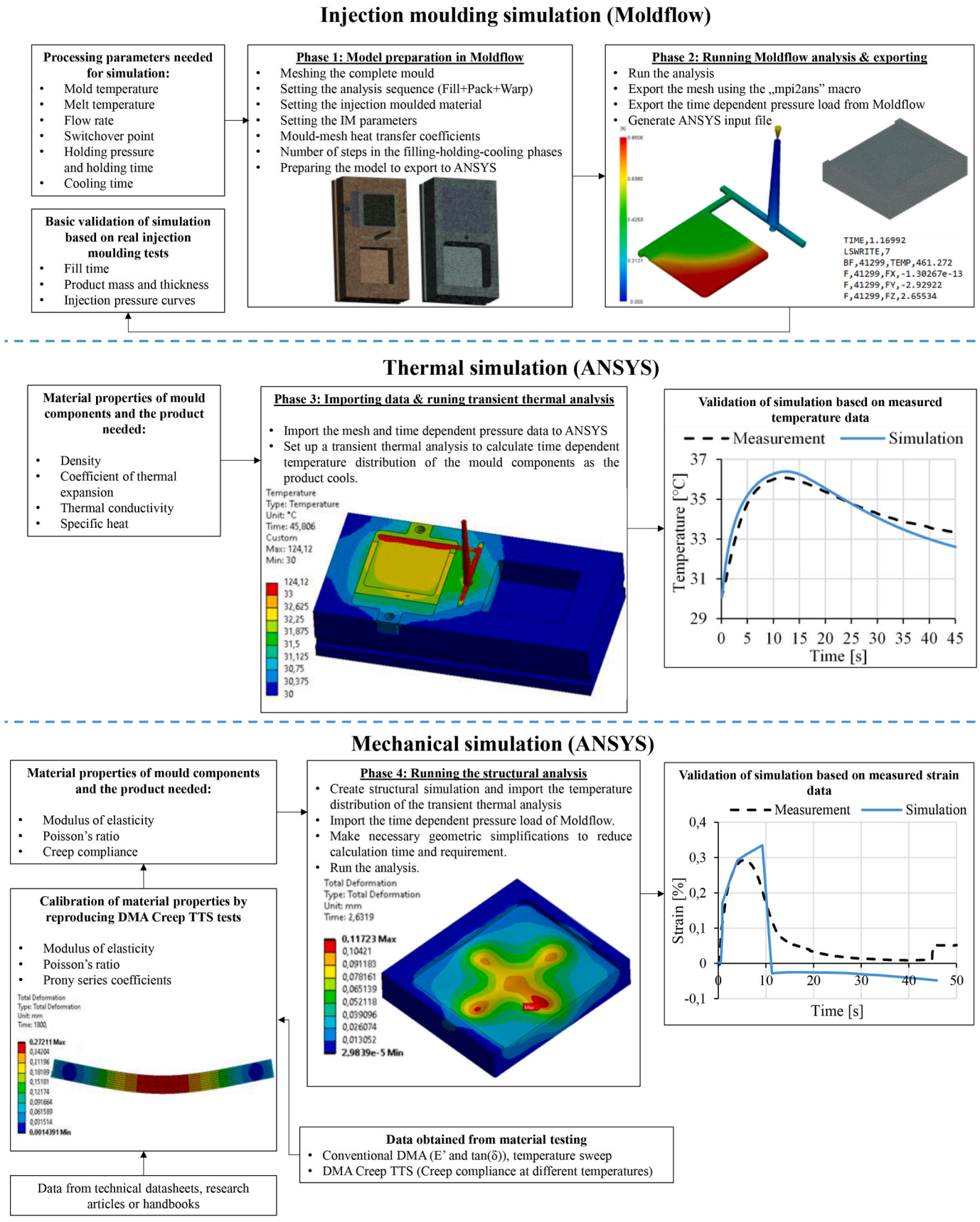

Fig. 10. Flowchart of the simulation process of polymeric mould inserts.

collected from material datasheets. Additional required inputs are the heat transfer coefficients between the mould components and the part, which require physical operational temperature measurement to be set correctly. The heat transfer coefficients were set to 300 W/(m^2•°C) for the contacts between the cavity walls and the product and to 1250 W/(m^2•°C) between the mould components. Actual operational temperature measurement is also necessary for the proper validation of the simulated temperature results. Validation with measurement is a prerequisite for the thermal simulation to provide acceptable results. Following the thermal simulation, the calculated time-dependent temperature field can be used as an input for the mechanical simulation. Mechanical modelling requires the modulus of elasticity, the Poisson's ratio and the creep compliance (in the case of polymeric mould inserts) of the analysed mould components. These data can be collected from literature, technical datasheets or they can be measured. In this case, we applied conventional DMA to measure the storage modulus, which we used to determine the temperature-dependent modulus of elasticity. We also carried out DMA Creep TTS tests to measure the creep compliance of the material and created a small model of the material test to calibrate the parameters of the viscoelastic material model.

3.4.1. Simulation of the creep behaviour of the material

We modelled the creep behaviour of the mould insert in Ansys Workbench using the Prony-series shear relaxation model. Finite element systems typically model the viscoelastic materials in the small strain region based on the generalized Maxwell model [45]. The constitutive equation of a viscoelastic material in the small strain region is the following:

$$\sigma = \int_0^t 2G(t-\tau) \bullet \frac{\partial \varepsilon_d}{\partial \tau} d\tau + I \bullet \int_0^t K(t-\tau) \bullet \frac{\partial \varepsilon_v}{\partial \tau} d\tau \tag{2}$$

Where:

σ Cauchy stress tensor, ε_d deviatoric part of the strain tensor, ε_v volumetric (hydrostatic) strain,

I unit tensor,$G(t)$ shear relaxation kernel function,

$K(t)$ bulk relaxation kernel function, t current time, τ past time.

The kernel functions of the shear relaxation modulus and the bulk relaxation modulus can be approximated with the Prony series. The two moduli can be given independently of one another.

$$G(t) = G_\infty + \sum_{i=1}^{N_G} G_i \bullet e^{-t/\tau_i{}^G} \tag{3}$$

$$K(t) = K_\infty + \sum_{i=1}^{N_K} K_i \bullet e^{-t/\tau_i{}^K} \tag{4}$$

where.

G_∞, K_∞ shear elastic modulus and bulk elastic modulus of the completely relaxed material (at t = ∞),

G_i, K_i ith shear elastic and bulk elastic component of the Prony series,

$\tau_i{}^G$, $\tau_i{}^K$ relaxation time of the ith component of the Prony series,

N_G, N_K number of Prony terms.

The initial shear modulus and bulk modulus can be derived by substituting t = 0 s into Eqs. (3)-(4)

$$G(t=0) = G_\infty + \sum_{i=1}^{N_G} G_i \tag{5}$$

$$K(t=0) = K_\infty + \sum_{i=1}^{N_K} K_i \tag{6}$$

The initial shear modulus and bulk modulus can be calculated by the formulae from elasticity:

$$G(t=0) = G_0 = \frac{E}{2 \bullet (1+\nu)} \tag{7}$$

$$K(t=0) = K_0 = \frac{E}{3 \bullet (1-2\nu)} \tag{8}$$

where: ν is the Poisson's ratio of the material.

We calculated the time-dependent creep modulus from the measured creep compliance at all analysed temperatures with the following formula:

$$E(t) = \frac{1}{J(t)} \tag{9}$$

Then, we converted the calculated creep modulus into shear modulus with the formula from elasticity:

$$G(t) = \frac{E(t)}{2 \bullet (1+\nu)} \tag{10}$$

We approximated the shear modulus with a four-term Prony-series at each temperature and validated the model by comparing the simulated crosshead displacement to the measured values. The mechanical model and the simulated displacement field is shown in Fig. 11. Supports were applied to prohibit deformation in the vertical (Z) direction indicated by the roller sliders in the figure.

The measured clamp displacements are compared to the simulated results in Fig. 12. Excellent agreements can be found between the measured data and the simulation in the analysed temperature region, covering the application temperature range of the mould insert. These agreements between the measured data and the simulation validate the modelling technique and prove its applicability.

3.4.2. Injection moulding simulation

The creep tests were successfully reproduced by simulation. After that, we created an injection moulding simulation model in Moldflow. We meshed the mould in Autodesk Moldflow Insight using 4-node tetrahedron elements. The mesh consisted of 675 791 nodes and 3 676 221 elements providing sufficient mesh density for the analysed regions (part and mould insert, especially around the cavity surface and the measurement locations of temperature and strain). Global edge length was 5 mm and a matching mesh setting was applied to ensure node-to-node contacts for the components. Additional mesh refinement was added to the cavity surfaces, the gate area and the measurement locations of the strain gauges and the thermocouple (Fig. 13). The mould insert mesh is shown separately in Fig. 16.

The analysis type was Fill + Pack + Warp. The injection moulding parameters were set in accordance with Table 3. The results were exported from Moldflow with the "mpi2ans" macro, which exports the mould mesh and the time-dependent pressure and temperature data. The results were calculated in 10 steps for filling, 10 steps for the holding phase and 3 steps for residual cooling time. The fill pattern of the injection moulding simulation is shown as a validation tool in Fig. 14. The simulation result is acceptable because it follows the fill pattern of the actual short-shot products and fill time is in agreement with the measurements. The short shot products are presented in Fig. 15 The injection moulding simulations were made for four holding pressures: 75, 150, 200 and 275 bar.

3.4.3. Transient thermal simulation

The meshed geometry was imported into Ansys Workbench and a Transient Thermal simulation was prepared to model the thermal state of the mould. Fig. 16 shows the imported geometry and the mould insert mesh. The temperature of the entire body of the injection moulded product was assumed to be the melt temperature throughout the filling phase (for 0.85 s). The product then cools down freely and the heat is transferred to the mould.

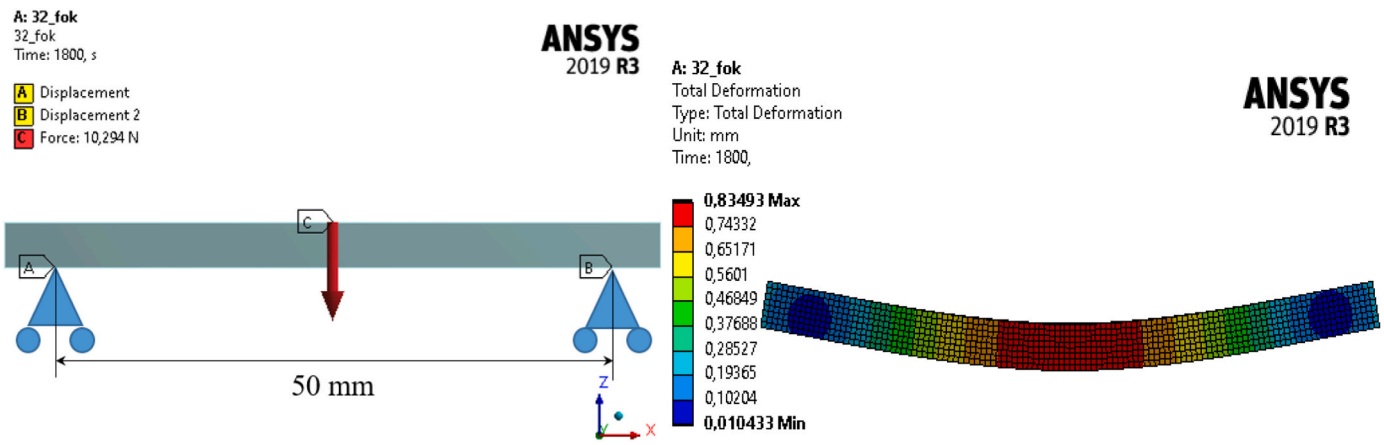

Fig. 11. The mechanical model of the Creep TTS tests and the deformed shape of the test specimen.

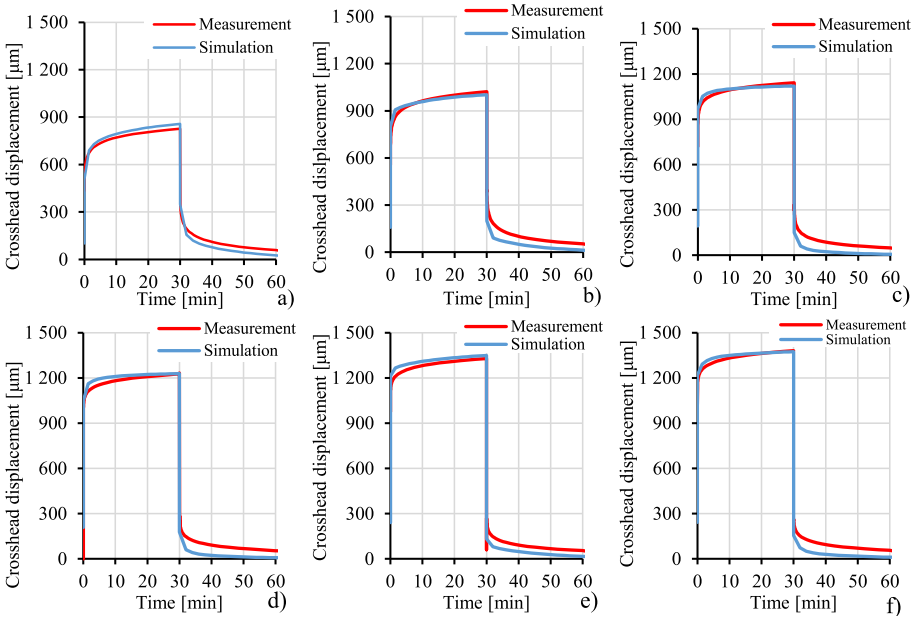

Fig. 12. Comparison of the measured clamp displacements with the finite element simulation results at 36, 45, 55, 65, 75 and 80 °C (from a) to f), respectively).

The temperature distribution around the mould insert is shown at characteristic time points in Fig. 17. The effect of the mould insert's low thermal conductivity can be clearly observed. The heated zone of the mould insert is localised strictly around the cavity surface and a significant temperature drop can be observed across the 6 mm thick wall. The spread of heat is very slow as the heated zone is still small even at the end of the cycle. Because of these, it is essential to run a transient thermal simulation first as the limited thermal conductivity causes an uneven temperature distribution inside the mould insert. The operational behaviour of the polymeric mould inserts can only be modelled accurately if the transient thermal simulation reproduces the real, time-dependent temperature field correctly. It is because the stiffness and the creep compliance of the polymeric mould inserts as well as their thermal expansion are fundamentally determined by their temperature.

The effect of the limited thermal conductivity is also shown in Fig. 18. The temperature was queried in the simulation at different time points along the wall thickness above the slot for the thermocouple. The cavity surface, directly in contact with the hot melt showed the highest temperature, which fell from 103 °C (at 7.75 s) to 63 °C (at 45.85 s, which is the time of mould opening). The temperature dropped sharply along the wall thickness throughout the entire analysed time window. The end of the analysed path (which is the slot of the thermocouple) only heats by approximately 2 °C, which is in sharp contrast with the temperature drop of the cavity surface, discussed earlier. As expected, these results confirm how a volumetric temperature measurement of polymeric mould inserts is necessary (e.g., for process control) but not satisfactory for advanced process monitoring, because the temperature of the cavity surface can be significantly higher during operation. It is desirable to have a thermal imaging camera image as well, because this way the temperature of the cavity surface can be monitored after mould opening. The temperature of the cavity surface during the injection moulding cycle cannot be measured, therefore the only way to get a good estimate of that is to have a thoroughly validated thermal simulation model.

The simulation results were validated in all cases. Fig. 19 shows the comparison of the measured temperature–time curves and the simulation results. Good agreements can be found between measurement and simulation with all of the analysed holding pressures: 75, 150, 200 and 275 bar.

3.4.4. *Static structural simulation*

A structural simulation model was built, after the successful

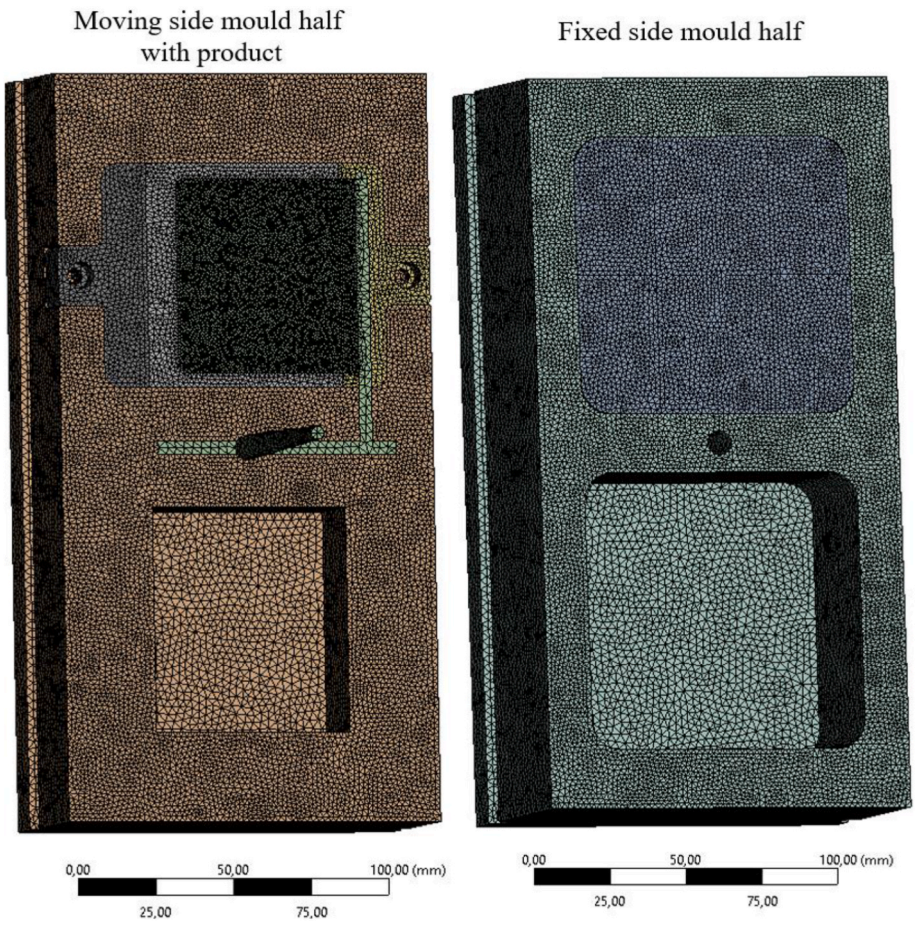

Fig. 13. Finite element mesh of the mould.

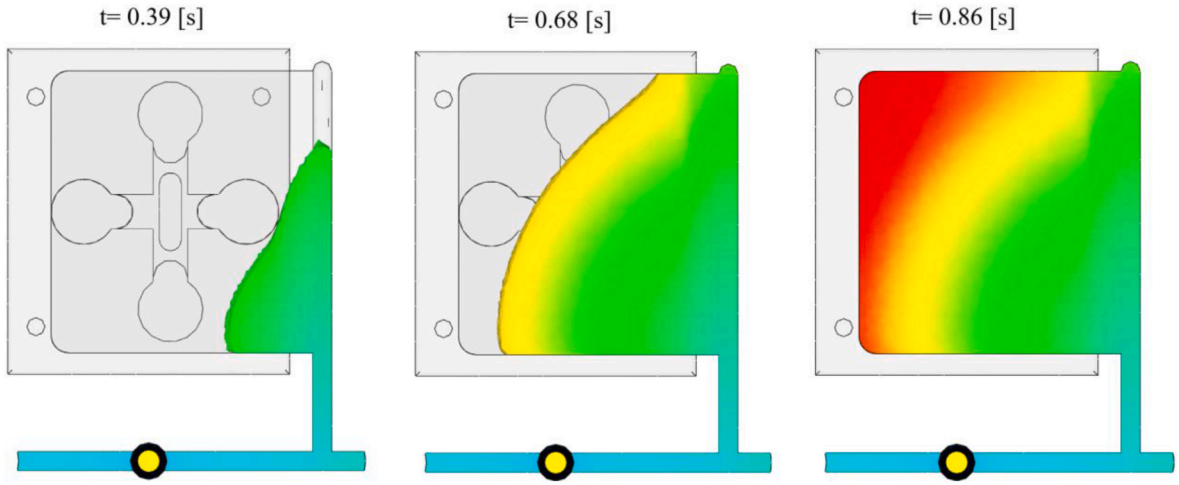

Fig. 14. The fill pattern of the injection moulded product.

validation of the results of the transient thermal simulation. The structural simulation requires the thermal field of the transient thermal simulation as an input. It also requires the Prony-series coefficients at the different temperatures, the modulus of elasticity and the Poisson's ratio (as functions of temperature). The modulus of elasticity in the simulations was determined based on the storage modulus measured by DMA (Fig. 2). The Prony-series coefficients were transferred from the creep models presented in Section 3.4.1 The time-dependent pressure load was imported from Moldflow as a list of nodal forces. We simplified the analysed geometry to reduce computation time and included only the moving side mould insert. The surfaces where the mould insert comes into contact with other mould components and the part were constrained by so-called "Compression-only supports". These supports simulate perfect contact with a completely rigid wall. The mould insert cannot cross this rigid wall but it can detach from it.

The total deformation of the mould insert is shown in Fig. 20 at the time when strain is maximal in the slot near the gate, at the four analysed holding pressures. The deformed shapes are in accordance with the

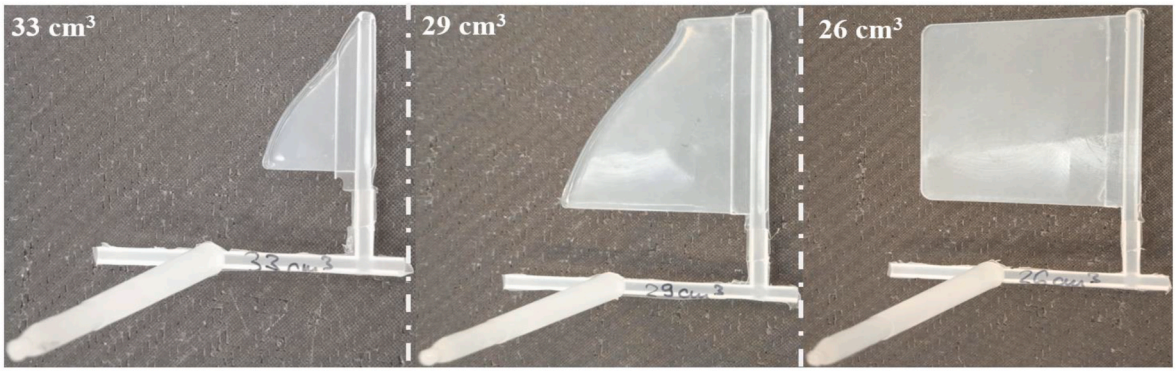

Fig. 15. The short shot products with their corresponding switchover volumes.

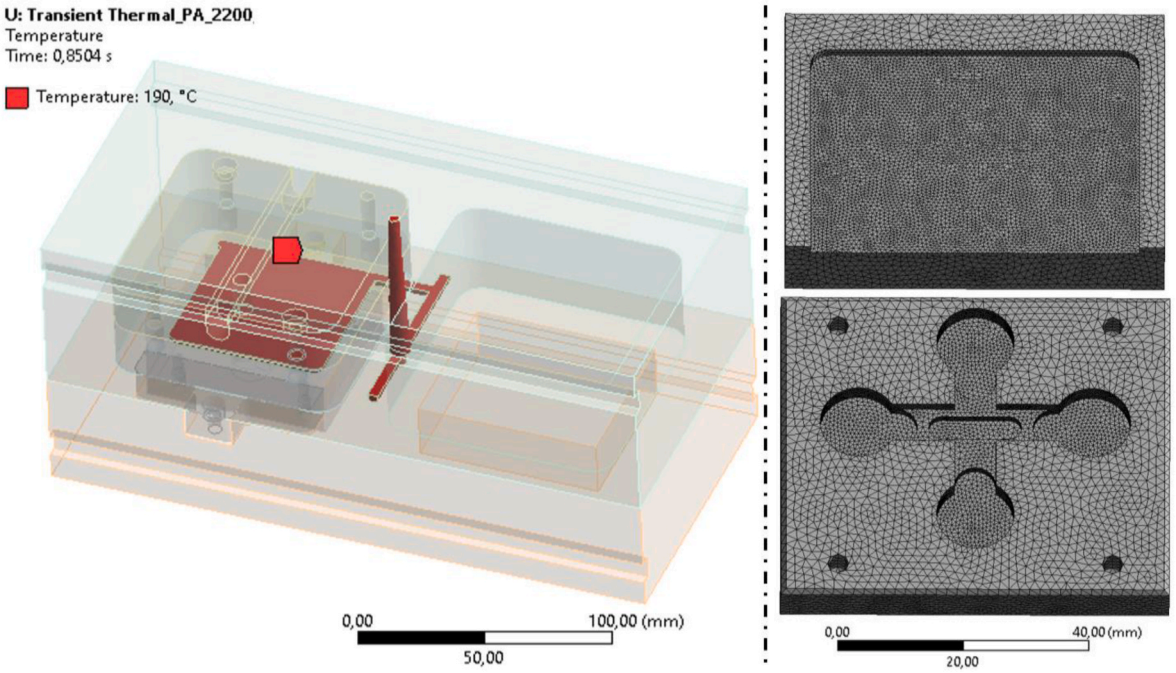

Fig. 16. The analysed geometry of the Transient thermal simulation and the mould insert mesh.

preliminary expectations as the slots bend under the pressure load acting on them. Other surfaces of the insert that are supported by the mould housing or the product cannot deform because of the Compression only supports. Deformation of the cavity surface is maximal above the slot near the gate, as the pressure load is higher there. Increasing the holding pressure also results in increasing mould deformations in a larger area of the cavity surface. It is in accordance with our preliminary expectations and the measured strains (Fig. 6). Maximal strain in the slot near the gate also occurs later, as holding pressure increases. It occurs right at switchover at a holding pressure of 75 bar, while it occurs approximately at the end of the holding phase at 275 bar. It is also in accordance with the results of the strain measurement (Fig. 6).

The mould deformation results were also validated with the operational strain measurements. Strain in the Y direction (in the coordinate system of Fig. 20) was compared to the measured strain (Fig. 21). Accuracy was good regarding both the maximal operational strain and the shape of the strain curves. These results prove that the presented coupled simulation approach can model both the thermal state and the deformational state of polymeric mould inserts with the required accuracy. It is of fundamental interest because polymeric moulds and part inserts for low-volume production are gaining considerable popularity in the injection moulding industry. The analysed phenomenon is quite complex because a mould insert made from a viscoelastic, non-linear material is subjected to a combined pressure and thermal load which is transient and also spatially varying. The accuracy of the simulations can be further improved by modelling the entire mould block and the product and not just the mould insert alone. This way, the finite rigidity of the surrounding components can also be considered in the model. However, it requires an excessive amount of calculation capacity, which is not necessarily needed for useable results. The presented model delivered accurate temperature and deformation results with a relatively low computational effort. The required level of accuracy always depends on the analyst's individual decision and the specific task.

4. Conclusions

In this article, we presented a novel coupled modelling approach to reproduce the operational behaviour of additively manufactured polymeric mould inserts. First, a comprehensive state monitoring system was presented for injection moulds that comprises operational strain, cavity pressure, volumetric temperature and surface temperature measurement. Material tests were carried out including conventional DMA and

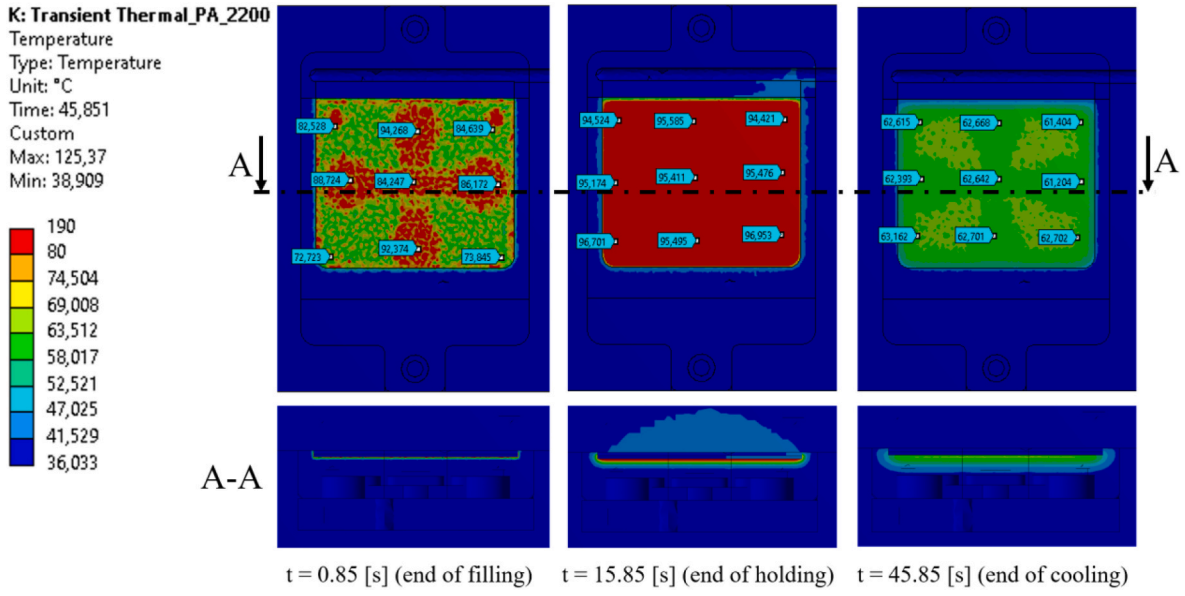

Fig. 17. Temperature distribution of the vicinity of the cavity at characteristic time points (end of filling, end of holding and end of cooling).

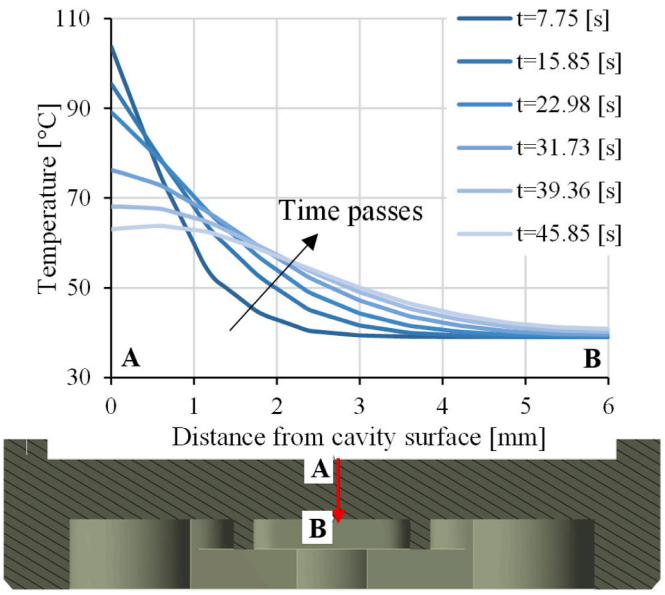

Fig. 18. Temperature distribution along the wall thickness of the mould insert at different time points.

creep testing to characterise the main mechanical parameters of the mould insert material needed for the simulations.

Following these preliminary tests, we performed the injection moulding test to measure the operational temperature and strain and to validate the simulation results.

After this, we outlined a novel simulation method, which is a combination of injection moulding simulation and finite element thermal and mechanical simulation. We presented a flowchart for that modelling method and listed the necessary parameters and the required supplementary tests. The presented simulation method starts with the reproduction of the creep tests by finite element mechanical simulation. We presented the Prony-series approximation of the shear elastic modulus, which can be applied to model the creep of the mould insert material. The creep tests were successfully reproduced indicated by the fact that the clamp displacements showed good agreements between the simulation and the experimental results. This validated creep model is a prerequisite of an acceptable mechanical simulation. Following that, we set up an injection moulding simulation in Autodesk Moldflow Insight, which is necessary to mesh the mould and to calculate the transient pressure and temperature fields during the injection moulding cycle. We validated this simulation model by comparing the fill pattern of the simulation with the actual short-shot products. After that, we exported the mould mesh and the time-dependent pressure and temperature data from Moldflow using the "mpi2ans" macro. These results were then imported to Ansys Workbench Mechanical, where a transient thermal

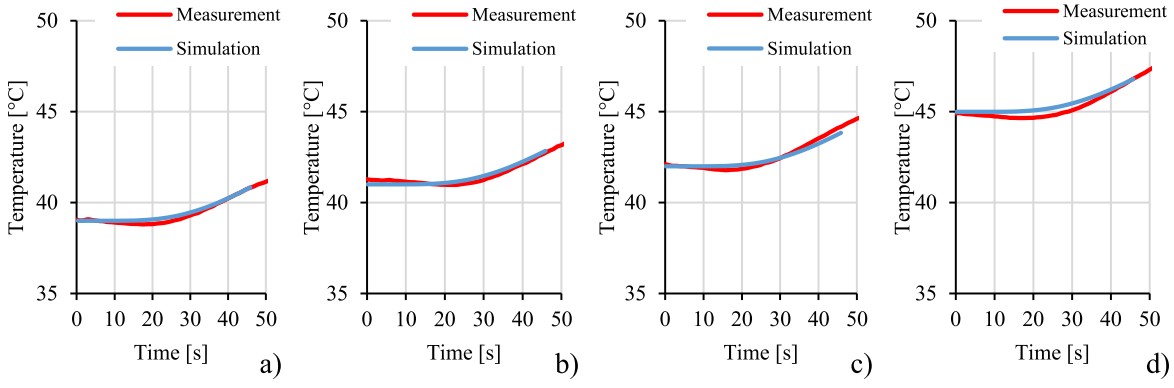

Fig. 19. The comparison of the measured and the simulated temperature curves at holding pressures of a) 75, b) 150, c) 200 and d) 275 bar.

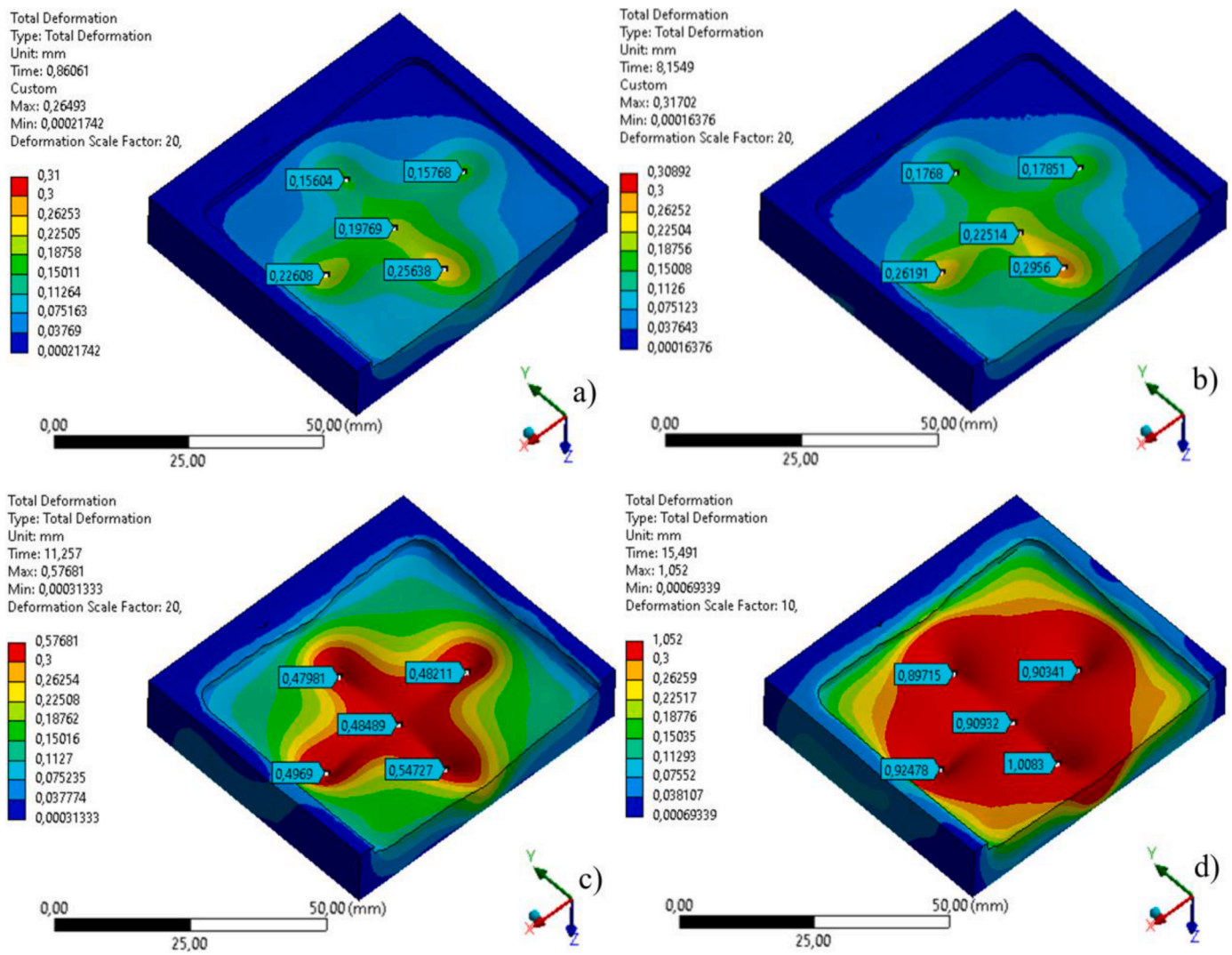

Fig. 20. The total deformation of the mould insert at the four analysed holding pressures a) 75, b) 150, c) 200, and d) 275 bar at the time of the maximal strain at the measured locations.

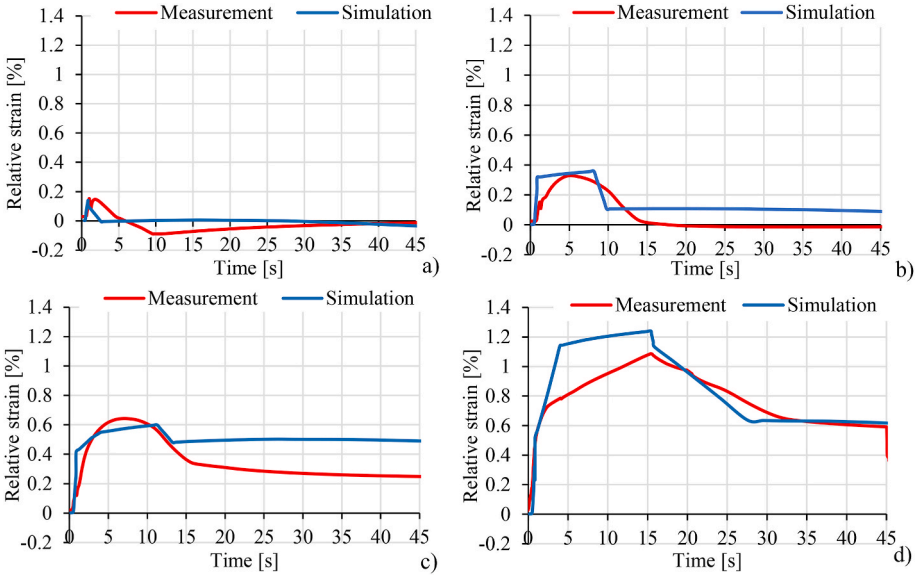

Fig. 21. The relative strain at the location near the gate of the mould insert at the four analysed holding pressures a) 75, b) 150, c) 200, and 275 bar.

analysis was set up. We simulated the cooling of the injection moulded product and the resulting temperature field in the surrounding mould components. The temperature results were validated for all four analysed holding pressures and excellent agreements were found between the measured temperature curves and the results of the thermal analysis. The transient temperature field was then linked to a static structural simulation that analysed the deformational state of the moving side mould insert during operation. The total deformation field of the mould insert was presented for all four analysed holding pressures and the results proved believable. The directional strain results were also queried in the simulation at the location of the strain gauges and were compared with the measured strain curves. The modelling method proved to be accurate because the measured and the simulated strain results showed good agreement. It has to be noted that this good agreement was reached with complex load and material properties. In this case, a spatially varying transient mechanical and thermal load is acting on a non-linear viscoelastic material. The simulation method outlined in this research paper was thoroughly validated with the state monitoring system and the supporting material tests. The presented simulation method can model the mechanical and thermal behaviour of polymeric moulds. This is of significant practical relevance because polymeric moulds and part inserts are gaining ground in the injection moulding industry. The presented simulation method allows a more systematic design and optimisation of these injection moulds and inserts in the future, which can bring increased production efficiency.

Funding

Project no. TKP-6-6/PALY-2021 has been implemented with the support provided by the Ministry of Culture and Innovation of Hungary from the National Research, Development and Innovation Fund, financed under the TKP2021-NVA funding scheme. Project no. RRF-2.3.1-21-2022-00009, titled National Laboratory for Renewable Energy has been implemented with the support provided by the Recovery and Resilience Facility of the European Union within the framework of Programme Széchenyi Plan Plus. This work was supported by the National Research, Development and Innovation Office, Hungary (FK 134336, FK 138501). This research was funded by the Horizon Europe Framework Programme and the call HORIZON-WIDERA-2021-ACCESS-03, under the grant agreement for project 101079051 – IPPT_TWINN. Sz. Krizsma is thankful for the support of the ÚNKP-23-3-II-BME-31 New National Excellence Program of the Ministry for Culture and Innovation from the source of the National Research, Development and Innovation Fund. Project no. KDP-IKT-2023-900-I1-00000957/0000003 has been implemented with the support provided by the Ministry of Culture and Innovation of Hungary from the National Research, Development and Innovation Fund, financed under the KDP-2023 funding scheme.

CRediT authorship contribution statement

Szabolcs Krizsma: Writing – original draft, Visualization, Validation, Methodology, Investigation, Data curation, Conceptualization. **Péter Széplaki:** Visualization, Validation, Investigation. **András Suplicz:** Writing – review & editing, Supervision, Methodology, Formal analysis, Conceptualization.

Declaration of competing interest

The authors declare that they have no known competing financial interests or personal relationships that could have appeared to influence the work reported in this paper.

Data availability

Data will be made available on request.

Acknowledgements

The authors wish to thank ARBURG HUNGÁRIA KFT. for the ARBURG Allrounder injection moulding machine, and TOOL-TEMP HUNGÁRIA KFT., LENZKES GMBH and PIOVAN HUNGARY KFT. for the accessories. We would like to thank the Faculty of Polymer Technology (FTPO, Slovenj Gradec, Slovenia) for printing the specimens and the mould insert.

References

[1] G. Tosello, A. Charalambis, L. Kerbache, M. Mischkot, D.B. Pedersen, M. Calaon, H. N. Hansen, Value chain and production cost optimization by integrating additive manufacturing in injection molding process chain, Int. J. Adv. Manuf. Technol. 100 (2019) 783–795, https://doi.org/10.1007/s00170-018-2762-7.
[2] S. Feng, A.M. Kamat, Y. Pei, Design and fabrication of conformal cooling channels in molds: review and progress updates, Int. J. Heat Mass Tran. 171 (2021) 121082, https://doi.org/10.1016/j.ijheatmasstransfer.2021.121082.
[3] C.-C. Kuo, Z.-F. Jiang, X.-Y. Yang, S.-X. Chu, J.-Q. Wu, Characterization of a direct metal printed injection mold with different conformal cooling channels, Int. J. Adv. Des. Manuf. Technol. 107 (2020) 1223–1238, https://doi.org/10.1007/s00170-020-05114-2.
[4] A. Kirchheim, Y. Katrodiya, L. Zumofen, F. Ehrig, C. Wick, Dynamic conformal cooling improves injection molding, Int. J. Adv. Des. Manuf. Technol. 114 (2021) 107–116, https://doi.org/10.1007/s00170-021-06794-0.
[5] M. Ben Slama, S. Chatti, A. Chaabene, K. Ghozia, H. Zamba Touati, Design for additive manufacturing of plastic injection tool inserts with maintenance and economic considerations: an automotive study case, J. Manuf. Process. 102 (2023) 765–779, https://doi.org/10.1016/j.jmapro.2023.07.070.
[6] I. Ilyas, C. Taylor, K. Dalgarno, J. Gosden, Design and manufacture of injection mould tool inserts produced using indirect SLS and machining processes, Rapid Prototyp. J. 16 (6) (2010) 429–440, https://doi.org/10.1108/13552541011083353.
[7] Y. Bai, Y. Yang, Z. Xiao, D. Wang, Selective laser melting of maraging steel: mechanical properties development and its application in mold, Rapid Prototyp. J. 24 (3) (2018) 623–629, https://doi.org/10.1108/RPJ-05-2017-0104.
[8] G. Dezső, F. Szigeti, G. Varga, Surface hardness modification of selective laser melted Ti6Al4V parts by sliding friction diamond burnishing, Period. Polytech. - Mech. Eng. 67 (1) (2023) 59–69, https://doi.org/10.3311/PPme.21124.
[9] D. Török, B. Zink, T. Ageyeva, I. Hatos, M. Zobač, I. Fekete, R. Boros, H. Hargitai, J. G. Kovács, Laser powder bed fusion and casting for an advanced hybrid prototype mold, J. Manuf. Process. 81 (2022) 748–758, https://doi.org/10.1016/j.jmapro.2022.07.034.
[10] A.B.M. Saifullah, S.H. Masood, I. Sbarski, Thermal–structural analysis of bi-metallic conformal cooling for injection moulds, Int. J. Adv. Des. Manuf. Technol. 62 (2012) 123–133, https://doi.org/10.1007/s00170-011-3805-5.
[11] J.A. Naranjo, C. Berges, R. Campana, G. Herranz, Rheological and mechanical assessment for formulating hybrid feedstock to be used in MIM & FFF, Results in Engineering 19 (2023) 101258, https://doi.org/10.1016/j.rineng.2023.101258.
[12] R. Alkentar, T. Mankovits, A study on the shape and dimensional accuracy of additively manufactured titanium lattice structures for orthopedic purposes, Period. Polytech. - Mech. Eng. 66 (4) (2022) 336–343, https://doi.org/10.3311/PPme.20382.
[13] B.R. Hunde, A.D. Woldeyohannes, Future prospects of computer-aided design (CAD) – a review from the perspective of artificial intelligence (AI), extended reality, and 3D printing, Results in Engineering 14 (2022) 100478, https://doi.org/10.1016/j.rineng.2022.100478.
[14] S.J. Park, J.H. Lee, J. Yang, W. Heogh, D. Kang, S.M. Yeon, S.H. Kim, S. Hong, Y. Son, J. Park, Lightweight injection mold using additively manufactured Ti-6Al-4V lattice structures, J. Manuf. Process. 79 (2022) 759–766, https://doi.org/10.1016/j.jmapro.2022.05.022.
[15] R. Mahshid, H.N. Hansen, K.L. Højbjerre, Strength analysis and modeling of cellular lattice structures manufactured using selective laser melting for tooling applications, Mater. Des. 104 (2016) 276–283, https://doi.org/10.1016/j.matdes.2016.05.020.
[16] D. Chantzis, X. Liu, D.J. Politis, Z. Shi, L. Wang, Design for additive manufacturing (DfAM) of hot stamping dies with improved cooling performance under cyclic loading conditions, Addit. Manuf. 37 (2021) 101720, https://doi.org/10.1016/j.addma.2020.101720.
[17] C. Tan, D. Wang, W. Ma, Y. Chen, S. Chen, Y. Yang, K. Zhou, Design and additive manufacturing of novel conformal cooling molds, Mater. Des. 196 (2020) 109147, https://doi.org/10.1016/j.matdes.2020.109147.
[18] G.A. Mendible, J.A. Rulander, S.P. Johnston, Comparative study of rapid and conventional tooling for plastics injection molding, Rapid Prototyp. J. 23 (2) (2017) 344–352, https://doi.org/10.1108/RPJ-01-2016-0013.
[19] P. Minetola, F. Calignano, M. Galati, Comparing geometric tolerance capabilities of additive manufacturing systems for polymers, Addit. Manuf. 32 (2020) 101103, https://doi.org/10.1016/j.addma.2020.101103.
[20] B. Zink, N.K. Kovács, J.G. Kovács, Thermal analysis based method development for novel rapid tooling applications, Int. Commun. Heat Mass Tran. 108 (2019) 104297, https://doi.org/10.1016/j.icheatmasstransfer.2019.104297.
[21] L. Giorleo, B. Stampone, G. Trotta, Micro injection moulding process with high-temperature resistance resin insert produced with material jetting technology:

effect of part orientation, Addit. Manuf. 56 (2022) 102947, https://doi.org/10.1016/j.addma.2022.102947.
[22] B. Stampone, K.I. Deniz, A. Foscarini, A. Turco, M.S. Chiriacò, F. Ferrara, L. Giorleo, G. Trotta, Rapid tooling for microinjection moulding of proof-of-concept microfluidic device: resin insert capability and preliminary validation, Appl. Sci. 14 (8) (2024) 3157, https://doi.org/10.3390/app14083157.
[23] A. Davoudinejad, M.R. Khosravani, D.B. Pedersen, G. Tosello, Influence of thermal ageing on the fracture and lifetime of additively manufactured mold inserts, Eng. Fail. Anal. 115 (2020) 104694, https://doi.org/10.1016/j.engfailanal.2020.104694.
[24] A. Bagalkot, D. Pons, D. Clucas, D. Symons, A methodology for setting the injection moulding process parameters for polymer rapid tooling inserts, Rapid Prototyp. J. 25 (9) (2019) 1493–1505, https://doi.org/10.1108/RPJ-10-2017-0217.
[25] Sz Krizsma, A. Suplicz, Comprehensive in-mould state monitoring of Material Jetting additively manufactured and machined aluminium injection moulds, J. Manuf. Process. 84 (2022) 1298–1309, https://doi.org/10.1016/j.jmapro.2022.10.070.
[26] Sz Krizsma, A. Suplicz, Analysis of the applicability and state monitoring of material extrusion–printed acrylonitrile butadiene styrene injection mould inserts with different infill levels, Mater. Today Commun. 35 (2023) 106294, https://doi.org/10.1016/j.mtcomm.2023.106294, 106294.
[27] F. Lupone, E. Padovano, M. Pietroluongo, S. Giudice, O. Ostrovskaya, C. Badini, Optimization of selective laser sintering process conditions using stable sintering region approach, Express Polym. Lett. 15 (2) (2021) 177–192, https://doi.org/10.3144/expresspolymlett.2021.16.
[28] T.L.A. Montanheiro, V.M. Schatkoski, B.R.C. de Menezes, B.R.C. Pereira, R. G. Ribas, R.G. de Freitas, A.P. Lemes, M.H.F. Fernandes, G.P. Thim, Recent progress on polymer scaffolds production: methods, main results, advantages and disadvantages, Express Polym. Lett. 16 (2) (2022) 197–219, https://doi.org/10.3144/expresspolymlett.2022.16.
[29] D. Soldner, S. Greiner, C. Burkhardt, D. Drummer, P. Steinmann, J. Mergheim, Numerical and experimental investigation of the isothermal assumption in selective laser sintering of PA12, Addit. Manuf. 37 (2021) 101676, https://doi.org/10.1016/j.addma.2020.101676.
[30] A. Salazar, A.J. Cano, J. Rodríguez, Mechanical and fatigue behaviour of polyamide 12 processed via injection moulding and selective laser sintering. Analysis based on Kitagawa-Takahashi diagrams, Eng. Fract. Mech. 275 (2022) 108825, https://doi.org/10.1016/j.engfracmech.2022.108825.
[31] A.A. Dastjerdi, M.R. Movahhedy, J. Akbari, Optimization of process parameters for reducing warpage in selected laser sintering of polymer parts, Addit. Manuf. 18 (2017) 285–294, https://doi.org/10.1016/j.addma.2017.10.018.
[32] A. Kampker, J. Triebs, S. Kawollek, P. Ayvaz, T. Beyer, Direct polymer additive tooling – effect of additive manufactured polymer tools on part material properties for injection moulding, Rapid Prototyp. J. 25 (10) (2019) 1575–1584, https://doi.org/10.1108/RPJ-07-2018-0161.
[33] C. Macedo, A.M. Brito, L. Faria, C.L. Simões, J. Laranjeira, R. Simoes, The potential of RHCM technology in injection molding using a simple convention heating and cooling system, Results in Engineering 19 (2023) 101349, https://doi.org/10.1016/j.rineng.2023.101349.
[34] F. Baruffi, M. Gülçür, M. Calaon, J.-M. Romano, P. Penchev, S. Dimov, B. Whiteside, G. Tosello, Correlating nano-scale surface replication accuracy and cavity temperature in micro-injection moulding using in-line process control and high-speed thermal imaging, J. Manuf. Process. 47 (2019) 367–381, https://doi.org/10.1016/j.jmapro.2019.08.017.
[35] R. Mahshid, Y. Zhang, H.N. Hansen, A.H. Slocum, Effect of mold compliance on dimensional variations of precision molded components in multi-cavity injection molding, J. Manuf. Process. 67 (2021) 12–22, https://doi.org/10.1016/j.jmapro.2021.04.048.
[36] Y. Zhao, P. Zhao, J. Zhang, J. Huang, N. Xia, J. Fu, On-line measurement of clamping force for injection molding machine using ultrasonic technology, Ultrasonics 91 (2019) 170–179, https://doi.org/10.1016/j.ultras.2018.08.013.
[37] M. Vukovic, S. Stemmler, K. Hornberg, D. Abel, C. Hopmann, Adaptive model-based predictive control for cross-phase cavity pressure control in injection molding, J. Manuf. Process. 77 (2022) 730–742, https://doi.org/10.1016/j.jmapro.2022.02.030.
[38] M. Kurt, O.S. Kamber, Y. Kaynak, G. Atakok, O. Girit, Experimental investigation of plastic injection molding: assessment of the effects of cavity pressure and mold temperature on the quality of the final products, Mater. Des. 30 (2009) 3217–3224, https://doi.org/10.1016/j.matdes.2009.01.004.
[39] P. Guerrier, G. Tosello, J.H. Hattel, Flow visualization and simulation of the filling process during injection molding, CIRP Journal of Manufacturing Science and Technology 16 (2017) 12–20, https://doi.org/10.1016/j.cirpj.2016.08.002.
[40] P. Guerrier, G. Tosello, K.K. Nielsen, J.H. Hattel, Three-dimensional numerical modeling of an induction heated injection molding tool with flow visualization, Int. J. Adv. Manuf. Technol. 85 (2016) 643–660, https://doi.org/10.1007/s00170-015-7955-8.
[41] G. Tosello, F.S. Costa, High precision validation of micro injection molding process simulations, J. Manuf. Process. 48 (2019) 236–248, https://doi.org/10.1016/j.jmapro.2019.10.014.
[42] A. Davoudinejad, M. Bayat, D.B. Pedersen, Y. Zhang, J.H. Hattel, G. Tosello, Experimental investigation and thermo-mechanical modelling for tool life evaluation of photopolymer additively manufactured mould inserts in different injection moulding conditions, Int. J. Adv. Des. Manuf. Technol. 102 (2019) 403–420, https://doi.org/10.1007/s00170-018-3163-7.
[43] B. Abbès, F. Abbès, H. Abdessalam, A. Upganlawar, Finite element cooling simulations of conformal cooling hybrid injection molding tools manufactured by selective laser melting, Int. J. Adv. Des. Manuf. Technol. 103 (2019) 2515–2522, https://doi.org/10.1007/s00170-019-03721-2.
[44] M. Mazur, P. Brincat, M. Leary, M. Brandt, Numerical and experimental evaluation of a conformally cooled H13 steel injection mould manufactured with selective laser melting, Int. J. Adv. Des. Manuf. Technol. 93 (2017) 881–900, https://doi.org/10.1007/s00170-017-0426-7.
[45] ANSYS Workbench Mechanical, Help- Chapter 4.9. Viscoelasticity, 2019.